



## New perspectives of $^{19}\text{F}$ MAS NMR in the characterization of amorphous forms of atorvastatin in dosage formulations

Jiri Brus<sup>a,\*</sup>, Martina Urbanova<sup>a</sup>, Ivana Sedenkova<sup>a</sup>, Hana Brusova<sup>b</sup>

<sup>a</sup> Institute of Macromolecular Chemistry, Academy of Sciences of the Czech Republic, Heyrovsky Sq. 2, 162 06 Prague 6, Czech Republic

<sup>b</sup> Zentiva K.S., U Kabelovny 130, 102 37 Prague 10, Czech Republic

### ARTICLE INFO

#### Article history:

Received 13 September 2010

Received in revised form 16 February 2011

Accepted 20 February 2011

Available online 26 February 2011

#### Keywords:

$^{19}\text{F}$  MAS NMR

Factor analysis

Polymorphism

Amorphous solids

Atorvastatin

Pharmaceuticals

### ABSTRACT

Despite recent advances in solid-state NMR spectroscopy, the structural characterization of amorphous active pharmaceutical ingredients (APIs) in solid dosage forms continues to be a monumental challenge. To circumvent complications following from low concentrations of APIs in tablet formulations, we propose a new time-saving procedure based on chemometric approach: factor analysis of  $^{19}\text{F}$  MAS NMR spectra. Capability of the proposed method is demonstrated on atorvastatin – a typical representative of fluorinated pharmaceutical substances exhibiting extensive polymorphism. Applying the factor analysis on the recorded  $^{19}\text{F}$  MAS NMR spectra, unique parameters for every sample were derived. In this way every solid form of atorvastatin was characterized and clearly distinguishable even among various amorphous and disordered forms. The proposed method was also found to be suitable for both qualitative and quantitative analysis of mixtures of various forms of atorvastatin. Reliability of the proposed method was extensively examined by comparing the obtained results with other experimental techniques such as  $^{13}\text{C}$  CP/MAS NMR, FTIR and XRPD. As highly linear correlations between the sets of parameters obtained from different experimental data were found, the perspectives of the applied comparative factor analysis to obtain detail structural view on variability of amorphous forms of atorvastatin are also discussed. Although the reported method was tested on atorvastatin, authors expect wider application for any fluorinated compound to give the routine, fast and reliable characterization of amorphous forms of APIs in drug products even at low concentrations (1–5%). Bear in mind that 20–25% of currently developed pharmaceuticals contain at least one fluorine atom in the molecule.

© 2011 Elsevier B.V. All rights reserved.

### 1. Introduction

In pharmaceutical development, amorphous forms of active pharmaceutical ingredients (APIs) currently attract significant attention (Zakrzewski and Zakrzewski, 2006). Amorphous or low-ordered systems show in general higher solubility but less stability in comparison to crystalline, well-ordered systems. Big challenge for solid-state analysis is thus to detect any change of manufactured amorphous form of the API, because the undesired structural changes can affect quality (properties of drugs) and also can lead to complicated patent litigations (Bauer et al., 2001; Blagden et al., 2007; Graeser et al., 2008; Greco and Bogner, 2010).

In general there is a wide range of physical methods suitable for characterization of pharmaceutical solids (Zakrzewski and Zakrzewski, 2006). X-ray powder diffraction (XRPD),  $^{13}\text{C}$  cross-

polarization (CP) magic-angle spinning (MAS) NMR and vibration spectroscopy are traditional tools to characterize typical well-ordered polymorphs (Brus and Jegorov, 2004; Harris, 2006, 2007; Harris et al., 2007; Husak et al., 2008, 2010), but sophisticated analytical tool to describe subtle differences between different amorphous forms of a particular API is still missing. In particular, in tablet formulations where concentrations of the API are very low and the strong signals of filler compounds dominate, we are balancing on physical and detection limits of conventional analytical methods. In these cases special techniques must be used (Griffin et al., 2007). That is why the characterization of amorphous forms of APIs and their unambiguous identification in tablet formulations is a priority that still remains a challenge.

In this context we see the potential of multivariate analysis of experimental data as a possible way to bridge this gap (Graeser et al., 2008; Heinz et al., 2008, 2009), especially in a combination with  $^{19}\text{F}$  MAS NMR spectroscopy (Aso et al., 2009; Harris, 2006). It has become evident that fluorinated compounds have a remarkable record in medicinal chemistry and will play an important role in providing lead compounds for therapeutic applications (Purser et al., 2008). Nowadays approximately 20–25% of drugs in the phar-

\* Corresponding author. Tel.: +420 296 809 380; fax: +420 296 809 410.

E-mail addresses: [brus@imc.cas.cz](mailto:brus@imc.cas.cz) (J. Brus), [urbanova@imc.cas.cz](mailto:urbanova@imc.cas.cz) (M. Urbanova), [sedenkova@imc.cas.cz](mailto:sedenkova@imc.cas.cz) (I. Sedenkova), [hana.brusova@zentiva.cz](mailto:hana.brusova@zentiva.cz) (H. Brusova).

maceutical pipeline contain at least one fluorine atom, and in 2007 nearly 50% of 20 best selling pharmaceutical products were based on fluorinated APIs. Consequently, the application of  $^{19}\text{F}$  MAS NMR spectroscopy in pharmaceutical research receives growing importance. The increasing interest also follows from high gyromagnetic ratio and 100% isotopic abundance of fluorine atoms ( $^{19}\text{F}$ ). Just this combination makes the  $^{19}\text{F}$  isotope to be one of the most sensitive NMR-active nuclei ever. The receptivity for  $^{19}\text{F}$  is 83% of that for  $^1\text{H}$ , and is 4700 times higher than that for  $^{13}\text{C}$ . Moreover, almost none of pharmaceutical excipients contain fluorine atoms. Therefore,  $^{19}\text{F}$  NMR spectra can be acquired very quickly even for diluted systems without the danger that  $^{19}\text{F}$  NMR signals of the API are overlapped by the signals of excipients.

On the other hand, there are still some limitations for fluorine NMR spectra to be generally used in characterizing amorphous solids. Predominantly the number of sites occupied by fluorine atoms in the molecules of common active substances is usually small.  $^{19}\text{F}$  MAS NMR spectra also remain poorly resolved even when measured at high spinning rates and at high magnetic fields.

A typical example of such behavior is currently the most produced drug – atorvastatin. This work, however, shows that even the poorly resolved  $^{19}\text{F}$  MAS NMR spectra of atorvastatin are sufficient to distinguish different amorphous forms of the given molecule, particularly when factor analysis (FA) is employed. As a consequence, subtle structural differences between different amorphous forms of atorvastatin are revealed and quantitative parameters identifying every form are provided. The ability of the proposed strategy to recognize various mixtures of amorphous forms is subsequently shown and the detection limits of minor components are discussed. Finally, the capability of the proposed strategy to characterize various low-ordered (amorphous) forms of atorvastatin in solid dosage formulations is demonstrated. In parallel, the proposed method is subjected to the extensive evaluation, validation. The results obtained by  $^{19}\text{F}$  MAS NMR spectroscopy are compared with structurally highly receptive experimental techniques like  $^{13}\text{C}$  CP/MAS NMR, FTIR and XRPD.

Overall, we tested potential of multivariate analysis of  $^{19}\text{F}$  MAS NMR spectra in terms of distinguishing different amorphous forms of both atorvastatin as a pure active pharmaceutical ingredient and atorvastatin as a low-concentration tablet formulation. As a result of this testing we suppose that the proposed strategy represents not only fast, routine and reliable tool to characterize amorphous forms of any fluorinated API in solid dosage forms, but also provides a new insight into the systems exhibiting extensive pseudopolymorphism or polymorphism for which high-resolution spectroscopic data cannot be obtained.

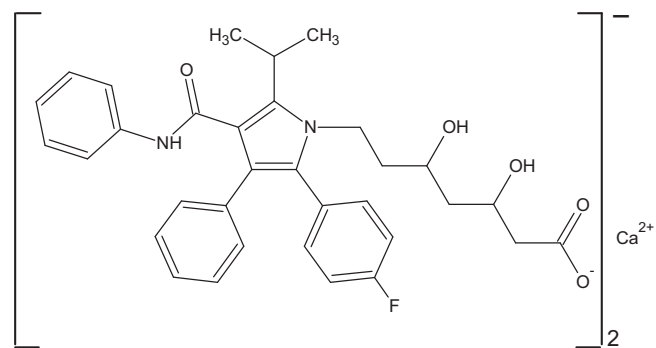
## 2. Materials and methods

### 2.1. Materials

Atorvastatin hemicalcium amorphous  $[(\text{C}_{33}\text{H}_{35}\text{FN}_2\text{O}_5^-)_2 \text{Ca}^{2+}]$  [Scheme 1] by Biocon Laboratories, Bangalore, India; Sucrose and Corn Starch by Sigma-Aldrich were used as received.

### 2.2. Methods: sample preparation – crystallization

Two spectroscopically well-defined highly crystalline forms and a wide range of amorphous (disordered, semicrystalline) modifications of atorvastatin hemicalcium were prepared according to the procedures described in literature (Aronhime et al., 2006; Ayalon et al., 2008; Briggs et al., 1999; Tessler et al., 2008). Following are the examples of the preparation of atorvastatin hemicalcium Form I, Form X and Form V, respectively: (i) 90 mg of atorvastatin hemicalcium as purchased was dissolved in hot water (9 ml,  $70^\circ\text{C}$ )



Scheme 1. Structural formula of atorvastatin.

and was allowed to stand 1 h at elevated temperature ( $70^\circ\text{C}$ ) and subsequently cooled down to room temperature. The crystals of the Form I were filtered out (Briggs et al., 1999). (ii) Form X was prepared by dissolving 90 mg of atorvastatin hemicalcium as purchased in a mixture of hot ethanol and water (10 ml,  $70^\circ\text{C}$ , wt. ratio 5:1) and was allowed to stand 2 h at elevated temperature ( $70^\circ\text{C}$ ) and subsequently cooled down to room temperature. The crystals of the Form X were filtered out (Tessler et al., 2008). (iii) Form V was prepared by dissolving 90 mg of atorvastatin hemicalcium as purchased in the mixture of hot methanol and water (10 ml,  $70^\circ\text{C}$ , wt. ratio 4:1) and was allowed to stand 3 h at elevated temperature ( $70^\circ\text{C}$ ) and subsequently cooled down to room temperature. The powders of the Form V were filtered out (Briggs et al., 1999). Other modifications of atorvastatin were prepared by similar procedures by dissolving of atorvastatin hemicalcium in various solvents such as methanol, water, ethanol, isopropanol, acetone, acetonitrile and mixtures thereof in varying proportions, at elevated temperature. The prepared solutions were allowed to stand at elevated temperature ( $70^\circ\text{C}$ ) in the range from 5 min to several hours and subsequently cooled down to room temperature. The obtained powders were filtered out. In all these cases dry powdered samples were used for further spectroscopic analysis without any purification. In summary, approximately 100 crystallization procedures were tested. In this way we tried to prepare as much forms of atorvastatin as possible to obtain a large set of different spectra for factor analysis. From all the prepared systems, the crystalline Forms I, V and X were unambiguously identified based on the  $^{13}\text{C}$  CP/MAS NMR and XRPD experimental data (Fig. 1, Briggs et al., 1999; Tessler et al., 2008). In general, however; we did not try to assign the prepared forms of atorvastatin to the products referred in patent literature, because it was not the purpose of our study. The unassigned amorphous modifications of atorvastatin hemicalcium are thus referred as Forms A1–An. The product directly received from the supplier is referred herein as Form A0.

### 2.3. Models of dosage forms

The models of dosage forms consisting of the prepared forms of atorvastatin (ca. 10 mg) and powdered Sucrose or Corn Starch (ca. 100–200 mg) were prepared by simple physical mixing. The resulting concentration of atorvastatin in the prepared models of low-dose formulations was about 1–10 wt.%.

### 2.4. NMR experiments

All NMR experiments were performed on a Bruker Avance 500 WB/US NMR spectrometer in 4-mm and 2.5-mm double-resonance probeheads at carrier frequencies 500.18, 470.35 and 125.78 MHz for  $^1\text{H}$ ,  $^{19}\text{F}$ , and  $^{13}\text{C}$  nuclei, respectively. Standard cross-polarization

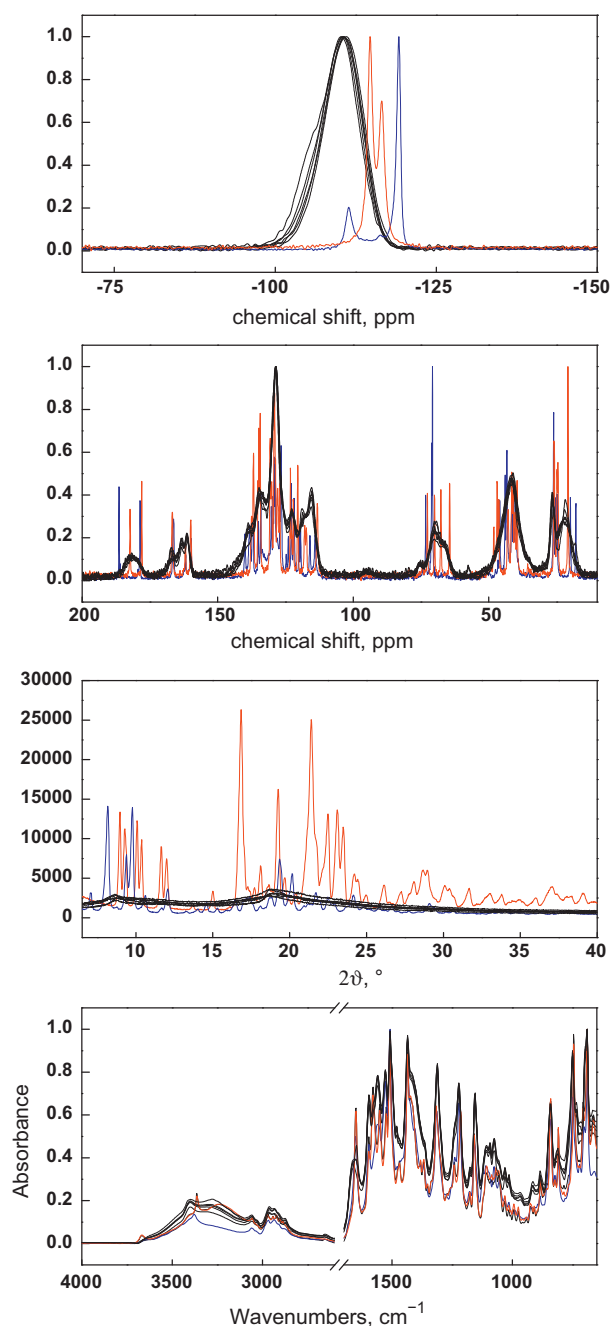


**Fig. 1.** Overlay of  $^{19}\text{F}$  MAS NMR,  $^{13}\text{C}$  CP/MAS NMR, XRPD patterns and FTIR spectra of the representative modifications of atorvastatin. The red lines mark crystalline Form I; the blue lines reflect crystalline Form X, and the black lines correspond to the amorphous forms of the API (A0–A7). (For interpretation of the references to color in this figure legend, the reader is referred to the web version of the article.)

experiments were used to record  $^{13}\text{C}$  CP/MAS NMR spectra at MAS frequency of 11 kHz (4-mm probehead, ca. 50 mg of the sample). The intensities of excitation and spin-locking fields  $B_1(^{13}\text{C})$  expressed in frequency units  $\omega_1/2\pi = \gamma B_1$  were 64 kHz and the duration of cross-polarization contact time pulse was 2 ms. The intensity of  $B_1(^1\text{H})$  field of TPPM (two-pulse phase-modulated) decoupling was  $\omega_1/2\pi = 89.3$  kHz. The repetition delay was 4 s. The acquisition time to record  $^{13}\text{C}$  CP/MAS NMR spectra of pure atorvastatin with acceptable signal-to-noise ratio was about 4.5 h. Overnight experiments were run to acquire  $^{13}\text{C}$  CP/MAS NMR spectra of the corresponding models of low-dose formulations. A rotor synchronized Hahn-echo pulse sequence was used to measure  $^{19}\text{F}$

MAS NMR spectra at MAS frequency of 31 kHz (2.5-mm probehead, ca. 8 mg of the sample). The length of  $90^\circ$  ( $^{19}\text{F}$ ) pulse was 2.5  $\mu\text{s}$ , repetition delay was 4 s and the number of scans was 124–256 and 512–1024 for pure atorvastatin and atorvastatin in models of low-dose formulations, respectively. Active cooling was used to compensate frictional heating of rotating samples (Brus, 2000). The total experimental time to acquire one  $^{19}\text{F}$  MAS NMR spectrum with acceptable signal-to-noise ratio was ca. 20 and 120 min, respectively.

## 2.5. IR experiments

The ATR FTIR spectra were recorded on Thermo Nicolet NEXUS 870 FTIR Spectrometer with a MCT detector. Single reflection ATR accessory Golden Gate (Specac, UK) with diamond crystal was used. Spectral resolution was  $4\text{ cm}^{-1}$  with 256 scans taken for each spectrum. Spectral region between  $1700$  and  $2600\text{ cm}^{-1}$  strongly affected by absorption of diamond ATR crystal were cut off. The spectra were normalized to compensate the variations of pressure between the sample and ATR crystal.

## 2.6. XRPD measurements

A Philips X'PERT PRO MPD PANalytical diffractometer (Almelo, The Netherlands) with  $\text{CuK}\alpha$  radiation (wavelength:  $1.542\text{ \AA}$ ) was used at 45 kV and 40 mA. Samples were scanned  $4$ – $40^\circ$   $2\theta$  with a step size  $0.01^\circ$   $2\theta$  and a step time 150 s. Results were analyzed using X'PERT HighScore Plus software.

## 2.7. Statistical analysis: factor analysis and spectral pretreatment

Factor analysis (FA) using the singular value decomposition (SVD) algorithm was performed to extract information from the experimental data obtained by  $^{19}\text{F}$  MAS NMR,  $^{13}\text{C}$  CP/MAS NMR, IR and XRPD data, and to visualize differences between amorphous forms of atorvastatin. Processing of spectral data was performed using Matlab program package. The following spectral range was subjected to the factor analysis:  $^{19}\text{F}$  NMR: from 50 to  $-200$  ppm,  $^{13}\text{C}$  NMR: from 200 to  $-50$  ppm; IR: from  $650$  to  $4000\text{ cm}^{-1}$ ; XRPD: from  $6$  to  $40^\circ$   $2\theta$ . All spectra were base-line corrected and normalized. Preparation and processing of a moderately sized data set containing ca. 40 spectra took about 10 min.

## 3. Results

### 3.1. Primary spectroscopic data

The potential of  $^{19}\text{F}$  MAS NMR spectroscopy in structural characterization of amorphous solids is demonstrated on atorvastatin, a moderately-sized compound exhibiting extensive polymorphism (Scheme 1). From 1985 to the end of 2006 there were registered 17 patents claiming 63 forms of atorvastatin (Aronhime et al., 2003, 2006; Ayalon et al., 2008; Briggs et al., 1999; Gogulapati et al., 2004; Tessler et al., 2008). These modifications include several highly crystalline forms like Form I (Briggs et al., 1999), Form VII (Aronhime et al., 2003) or Form X (Tessler et al., 2008), and more than 50 disordered (semicrystalline, almost-amorphous and amorphous) forms [e.g. Form V (Briggs et al., 1999)]. As this substance contains one fluorine atom in its molecule – the fluorine is located in *para* position of the aromatic ring (Scheme 1) – atorvastatin represents an ideal system that can be used to explore explanatory power of  $^{19}\text{F}$  MAS NMR spectroscopy.

In the first step of our study, we explored structural receptivity of  $^{19}\text{F}$  MAS NMR spectra (Fig. 1). In order to maintain adequate clarity of the obtained results, this part of our investigation was

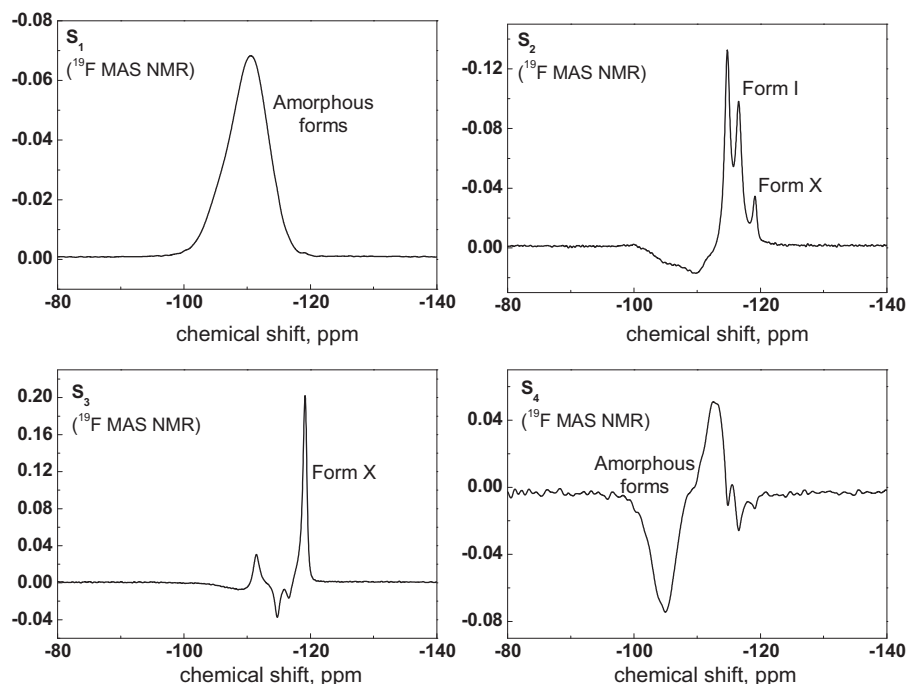


**Fig. 2.** Subspectra  $S_1(^{19}\text{F})$  to  $S_4(^{19}\text{F})$  obtained by the factor analysis of  $^{19}\text{F}$  MAS NMR spectra of the representative modifications of atorvastatin (see Appendix A, A1a and A1b, where singular values  $w_j(^{19}\text{F})$  and other high-order subspectra  $S_j(^{19}\text{F})$  are presented).

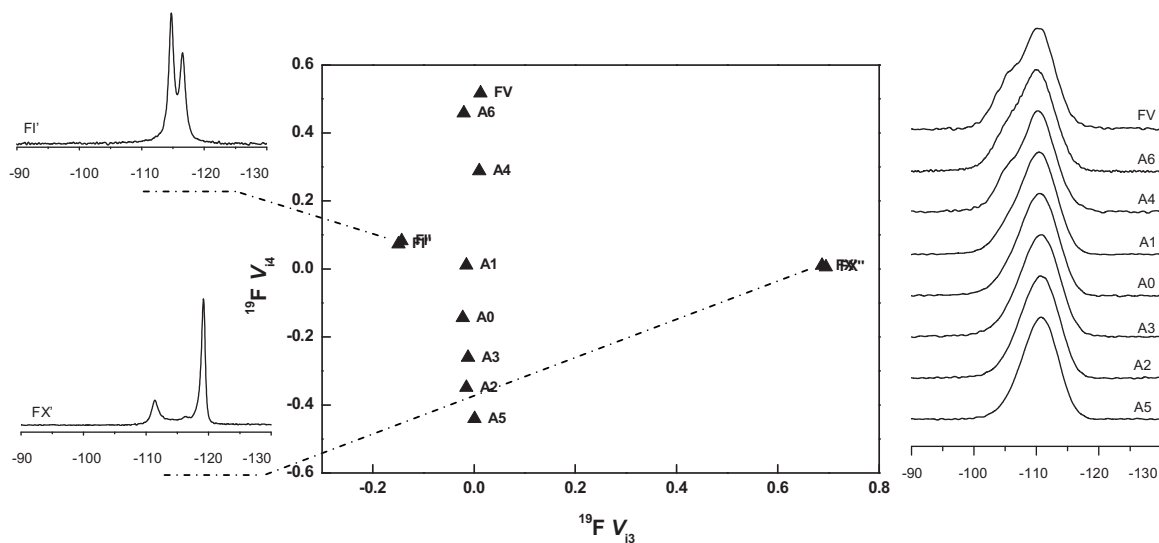


**Fig. 3.** Correlation plot of  $V_{13}(^{19}\text{F})$  and  $V_{14}(^{19}\text{F})$  coefficients. The coefficients were obtained by the factor analysis of  $^{19}\text{F}$  MAS NMR spectra of the representative modifications of atorvastatin. The corresponding  $^{19}\text{F}$  MAS NMR spectra of crystalline and amorphous modifications are placed on the left and right side, respectively.

conducted on a relatively small set of representative forms of atorvastatin which did not contain filler compounds. The selected set of the samples consisted of well-ordered crystalline Forms I and X; several amorphous forms prepared by us (thereafter referred as Form V and Forms A1–A7); and the sample received from the supplier (Form A0). For the purpose of this paper, the term “amorphous form” is used to refer both amorphous and disordered (partially crystalline) forms of atorvastatin.

In the recorded  $^{19}\text{F}$  MAS NMR spectra (Fig. 1) the crystalline modifications of atorvastatin (Form I and Form X) can be easily identified and distinguished from the amorphous ones (Forms V and A1–A7). This follows from the fact that the highly ordered crystalline forms produce narrow and well-resolved NMR signals,

while the amorphous ones give a single broad NMR signal. The obtained experimental data also reflect slight structural variations between the amorphous products of atorvastatin (Fig. 1). However, the spectral differences between them are not easy to find and quantitatively describe. Although this is the common problem of all spectroscopic data including XRPD, FTIR and  $^{13}\text{C}$  CP/MAS NMR (Fig. 1), the  $^{19}\text{F}$  MAS NMR spectra exhibit remarkably weakest spectral differences. As the spectral differences between the amorphous modifications of atorvastatin are very subtle, visual inspection of  $^{19}\text{F}$  MAS NMR spectra is not enough. Correct and rigorous interpretation of the observed variations of the  $^{19}\text{F}$  MAS NMR spectra thus requires special statistical processing based on factor analysis.

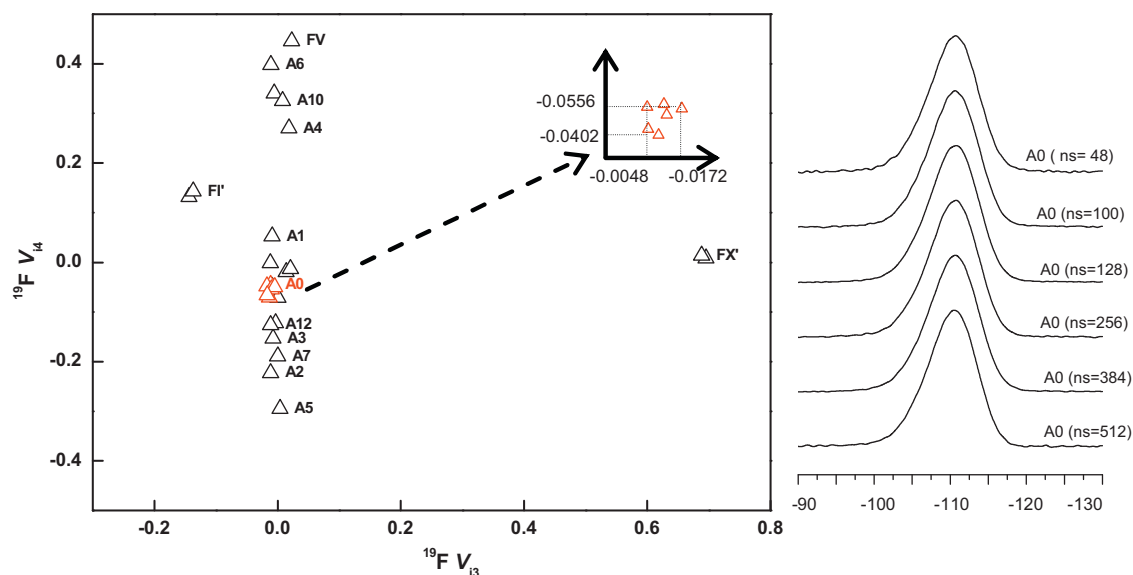


**Fig. 4.** Correlation plot of  $V_{13}(^{19}\text{F})$  and  $V_{14}(^{19}\text{F})$  coefficients. The coefficients were obtained by factor analysis of the extended set of  $^{19}\text{F}$  MAS NMR spectra of the representative modifications of atorvastatin. The  $^{19}\text{F}$  MAS NMR spectra of amorphous Form A0 recorded repeatedly over one week are placed on the right side. The expanded region of the correlation plot reflecting scatter of  $V_{ij}$  coefficients of A0 samples (read dots) is placed in the upper right corner.

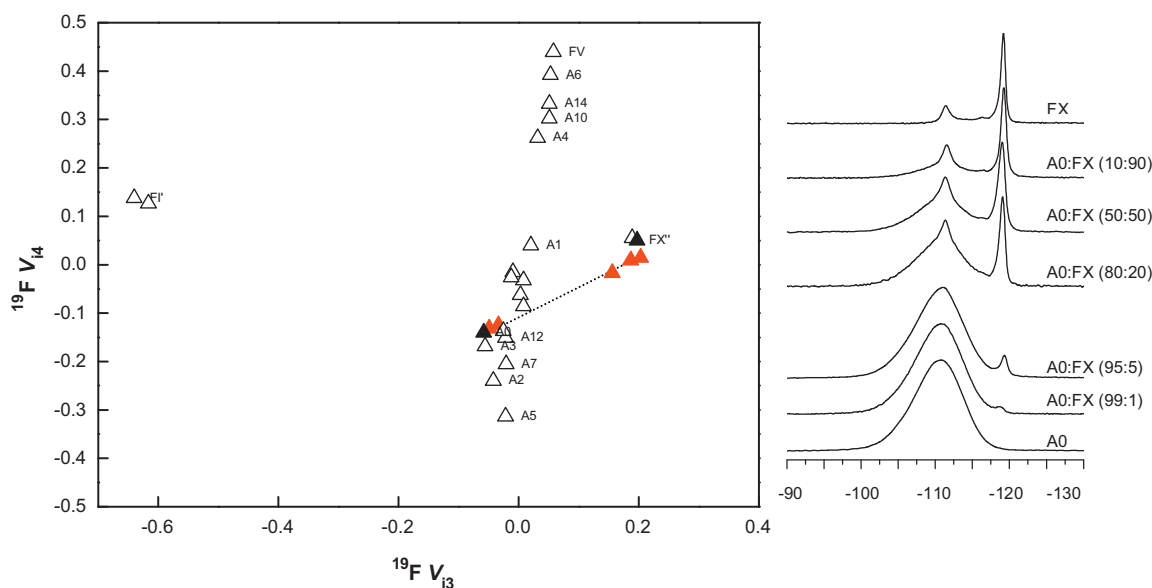


**Fig. 5.** Correlation plot of  $V_{13}(^{19}\text{F})$  and  $V_{14}(^{19}\text{F})$  coefficients. The coefficients were obtained by the factor analysis of the extended set of the  $^{19}\text{F}$  MAS NMR spectra of representative forms of atorvastatin. Red dots correspond with the crystalline–amorphous mixtures consisting of Form X and Form A0. The corresponding  $^{19}\text{F}$  MAS NMR spectra are placed on the right side. (For interpretation of the references to color in this figure legend, the reader is referred to the web version of the article.)

### 3.2. Factor analysis

In general, factor analysis (FA) provides a versatile tool to explore complex changes in large sets of experimental data (Claydenaq et al., 1997; Eads et al., 2004; Henry and Hofrichter, 1992; Koonst and Ellis, 1995; Levine, 1998). Specifically, the experimental spectra  $Y_i$  are converted into the set of orthonormal subspectra  $S_j$  (Eq. (1)) using singular value decomposition (SVD) algorithm.

$$Y_i = \sum_{j=1}^n w_j V_{ij} S_j \quad (1)$$

The calculated subspectra are linear combinations of the experimental data ( $n$  – number of experimental spectra) and *vice versa*

the experimental data can be given as the linear combination of the subspectra (Eq. (1)). Each subspectrum  $S_j$  represents a specific spectral feature that is typical for a given type of analyzed samples. The statistical importance and hence the order of each subspectrum  $S_j$  is expressed by the singular value,  $w_j$ . Significantly, the ability of a particular subspectrum  $S_j$  to describe the experimental spectrum  $Y_i$  is expressed by the normalized coefficient  $V_{ij}$ . Consequently the coefficients  $V_{ij}$  (i.e. scores) represent quantitative parameters reflecting spectral differences between the analyzed samples. In this way any modification of a particular API can be unambiguously identified via the set of  $V_{ij}$  coefficients. In this way, the large set of experimental data can be reduced into just several ( $m$ ,  $m < n$ ) essential factors (subspectra) that are sufficient to appropriate description of the experimental data series when only the subspectra associated with the highest singular values ( $w_j$ ) are taken to approximation.

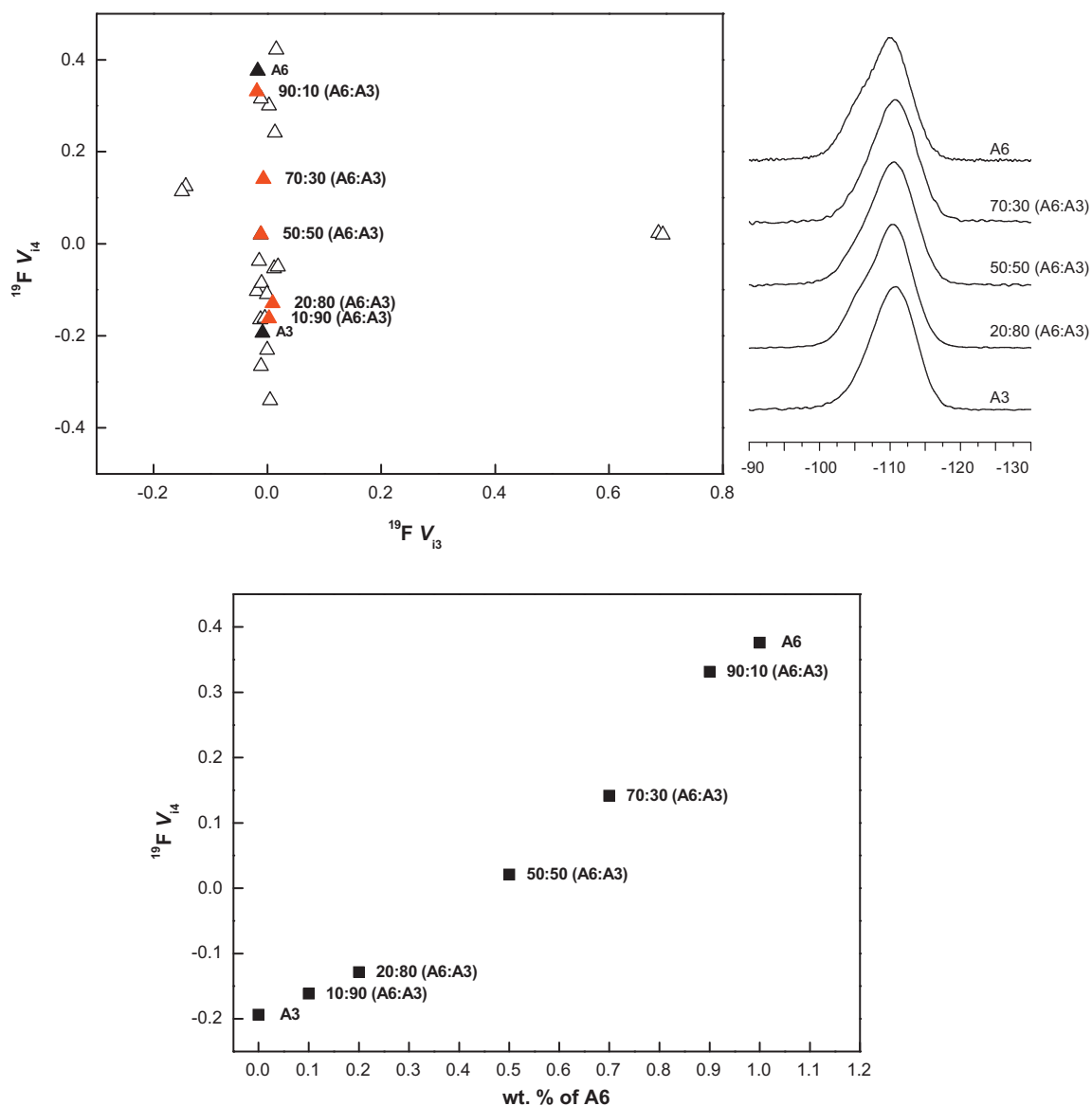


**Fig. 6.** Correlation plot of  $V_{13}(^{19}\text{F})$  and  $V_{14}(^{19}\text{F})$  coefficients. The coefficients were obtained by the factor analysis of the extended set of the  $^{19}\text{F}$  MAS NMR spectra of the representative modifications of atorvastatin. Red dots correspond to the scores of amorphous–amorphous mixtures consisting of Form A6 and Form A3. The relevant  $^{19}\text{F}$  MAS NMR spectra are placed on the right side. The dependence of  $V_{14}(^{19}\text{F})$  factors on the composition of analyzed mixtures (Form A6/Form A3) is depicted on the bottom chart. (For interpretation of the references to color in this figure legend, the reader is referred to the web version of the article.)

### 3.3. Factor analysis of $^{19}\text{F}$ MAS NMR spectra

Applying this statistical data treatment procedure, the recorded  $^{19}\text{F}$  MAS NMR spectra of atorvastatin were analyzed and the set of subspectra  $S_j(^{19}\text{F})$  together with their corresponding singular values  $w_j(^{19}\text{F})$  were derived. As only the singular parameters  $w_1(^{19}\text{F})$  to  $w_4(^{19}\text{F})$  reached reasonable values (Appendix A and A1a) the analyzed dataset is almost completely described by the corresponding subspectra  $S_1(^{19}\text{F})$  to  $S_4(^{19}\text{F})$  (Fig. 2). Other high-order subspectra  $S_5(^{19}\text{F})$  to  $S_n(^{19}\text{F})$  then reflect random variations in the electronic noise. Interpreting the obtained results, the 1st-order subspectrum  $S_1(^{19}\text{F})$  shows the mean signal representing the whole set of analyzed samples. In our particular case this mean signal resembles typical signal of amorphous forms of atorvastatin. The 2nd- and 3rd-order subspectra then depict specific markers of crystalline Forms I and X. The 3rd-order subspectrum  $S_3(^{19}\text{F})$  can also be interpreted as a difference spectrum reflecting spectral differences between the crystalline forms of atorvastatin. The spectral regions

in which the amorphous forms of the API differ from each other are highlighted in the 4th-order subspectrum  $S_4(^{19}\text{F})$ .

As follows from the above-mentioned interpretations, structural differences between the crystalline forms of atorvastatin can be explicitly expressed by the factors  $V_{13}(^{19}\text{F})$ , while the subtle differences between the amorphous forms are preferably described by  $V_{14}(^{19}\text{F})$  coefficients. In a graphical representation (one of the most suitable representation seems to be the correlation plot of  $V_{13}$  and  $V_{14}$  coefficients, Fig. 3) the crystalline Forms I and X are clearly separated in the horizontal dimension, while the amorphous forms (A0–A7) are vertically sorted. The observed systematic array of  $V_{14}(^{19}\text{F})$  coefficients clearly reflects differences between the amorphous forms of atorvastatin. Moreover, the considerably wide range of  $V_{14}(^{19}\text{F})$  values covering the interval from  $-0.5$  to  $0.5$  confirms the high structural receptivity of this parameter.

In order to verify reproducibility of the obtained results, the measurements of  $^{19}\text{F}$  MAS NMR spectra including their processing and SVD analysis were repeated. Over a short period the

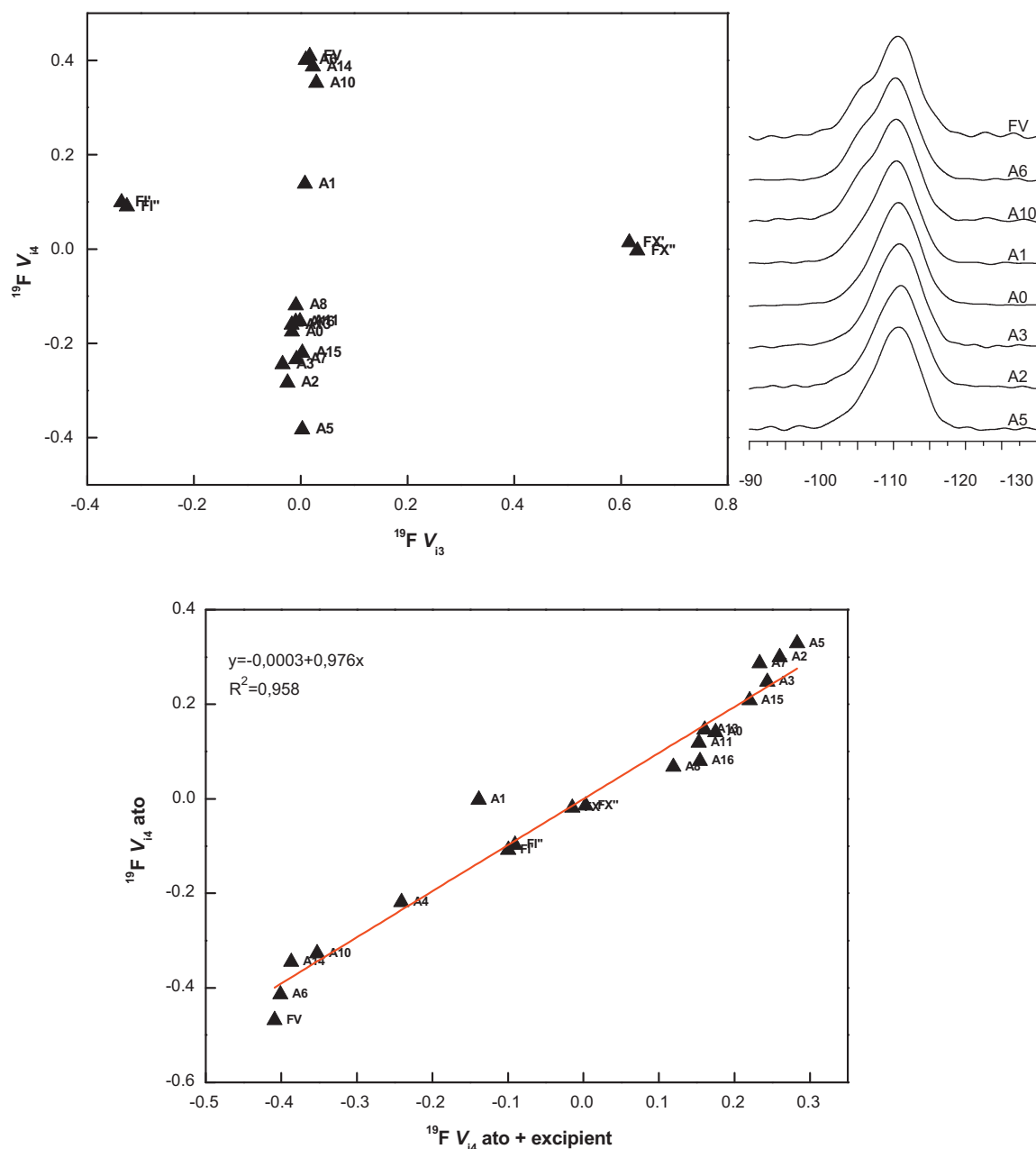


**Fig. 7.** Correlation plot of  $V_{13}(^{19}\text{F})$  and  $V_{14}(^{19}\text{F})$  coefficients. The coefficients were obtained by the factor analysis of  $^{19}\text{F}$  MAS NMR spectra of representative modifications of atorvastatin in mixtures with excipients. The corresponding  $^{19}\text{F}$  MAS NMR spectra of crystalline and amorphous forms are placed on the left and right side, respectively. The correlation of  $V_{14}(^{19}\text{F})$  parameters obtained for pure forms of the API and their corresponding low-dose model formulations.

$^{19}\text{F}$  MAS NMR spectra of selected samples were recorded several times at the same experimental conditions. In addition, to estimate the influence of electronic noise on the quality of the obtained results the number of scans accumulated to acquire one  $^{19}\text{F}$  MAS NMR spectrum was systematically varied. The obtained experimental data were subsequently processed by the factor analysis and  $V_{13}(^{19}\text{F})$ – $V_{14}(^{19}\text{F})$  correlation plots were created. In both tests no changes in relative displacement of  $V_{ij}(^{19}\text{F})$  parameters were observed in the resulting correlation plots. The calculated standard deviation of  $V_{13}(^{19}\text{F})$  scores was  $X = 4.23 \times 10^{-3}$  and  $Y = 9.36 \times 10^{-3}$  of  $V_{14}(^{19}\text{F})$  parameters resulting from 6 repetitions for a given sample (Fig. 4). Therefore it is clear that the proposed procedure is sufficiently robust and stable, and different forms of atorvastatin are unambiguously identified if the differences in their  $V_{ij}(^{19}\text{F})$  parameters exceed ca. two-times the above-mentioned standard

deviations. In addition, new measurements needed for the reproducibility test significantly enlarged the dataset of processed  $^{19}\text{F}$  MAS NMR spectra up to 50 analyzed forms of atorvastatin in total. When we compare the original data set (Fig. 3) and the new dataset including multiple measurement of one specie (e.g. Fig. 4), the resulting pattern of the obtained  $V_{13}(^{19}\text{F})$ – $V_{14}(^{19}\text{F})$  correlation plots remains practically unchanged. This indicates that factor analysis of  $^{19}\text{F}$  MAS NMR spectra provides self-consistent results that are basically independent on the number of processed experimental data and multiple presence of one amorphous form.

### 3.4. Two-component mixtures and detection limits

For several reasons, including stability and patenting issues, it is important to be able to ensure that, whichever solid-state form is

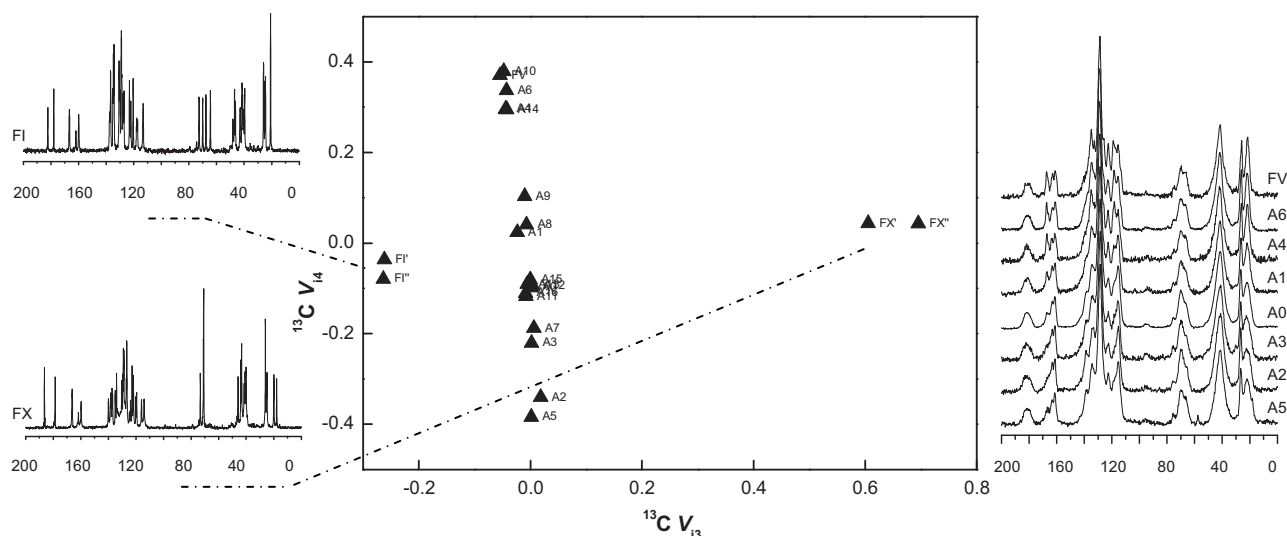


**Fig. 8.** Correlation plot of  $V_{13}(^{13}\text{C})$  and  $V_{14}(^{13}\text{C})$  coefficients. The coefficients were obtained by the factor analysis of  $^{13}\text{C}$  CP/MAS NMR spectra of the representative forms of atorvastatin. The corresponding  $^{13}\text{C}$  CP/MAS NMR spectra of crystalline and amorphous forms are placed on the left and right side, respectively.

chosen, this form is not transformed or contaminated by other solid state forms. That is why an important question that often bothers pharmaceutical companies concerns the detection limits of minor components in the mixtures of various polymorphs. In this context we prepared and analyzed a wide range of two-component systems (crystalline–amorphous and amorphous–amorphous) in the weight ratio ranging from 1:99 to 99:1. It was found out that the presence of 1% of crystalline form of atorvastatin (e.g. Form I, Form X) dispersed in the amorphous matrix of atorvastatin (e.g. Forms A0–A6) can be easily detected. The recorded  $^{19}\text{F}$  MAS NMR spectra as well as the calculated  $V_{13}(^{19}\text{F})$  or  $V_{14}(^{19}\text{F})$  coefficients differ from those obtained for pure forms (Fig. 5). On the other hand, the lowest amount of an amorphous form of atorvastatin (e.g. Forms A0–A6) that can be clearly detected in the crystalline matrix of atorvastatin (Forms I and X) is higher than in the previous case, and it is at least 5–10%. This is the lowest amount of the amorphous fraction of atorvastatin that induces distinct changes in  $V_{13}(^{19}\text{F})$  and  $V_{14}(^{19}\text{F})$  coefficients (Fig. 5). Smaller amounts are under the limit of detection (LOD).

The situation is a bit more complicated in the mixtures consisting of two amorphous forms of the API. It was found out that in some cases just the presence of approximately 5–10 wt.% of a minor component can induce changes in  $^{19}\text{F}$  MAS NMR spectra that can be recognized by the factor analysis. It is worth noting that the values of  $V_{14}(^{19}\text{F})$  coefficients representing the two-component mixtures systematically move towards the center of the region that is limited by  $V_{14}(^{19}\text{F})$  scores of both pure forms of atorvastatin (Fig. 6). As the obtained scores almost linearly vary with the composition of the analyzed mixtures, the calibration curves describing particular two-component systems can be also created.

### 3.5. Effect of filler compounds in low-dose model formulations of atorvastatin

So far, the proposed method has been tested on the systems of pure atorvastatin without filler compounds. The real application in pharmaceutical research, however, strongly depends on the ability to detect, identify and distinguish different amorphous forms of the API in low-dose tablet formulations. That is why a large collection of models of low-dose formulations (mixtures with filler compounds) containing approximately 1–5 wt.% of atorvastatin was prepared and a new dataset of  $^{19}\text{F}$  MAS NMR spectra was created. Subsequently, the recorded  $^{19}\text{F}$  MAS NMR spectra of these systems were

processed by the factor analysis. The resulting subspectra as well as characteristic features of  $V_{13}(^{19}\text{F})$ – $V_{14}(^{19}\text{F})$  correlation plot are quite comparable with the previous results keeping thus distinct vertical ordering of the amorphous forms and horizontal separation of crystalline forms of atorvastatin (compare Fig. 7 and Fig. 4). The high degree of congruence between these two sets of experimental data is demonstrated on the correlation plot of  $V_{14}(^{19}\text{F})$  scores obtained for pure forms of atorvastatin and the corresponding models of dosage formulations (Fig. 7, bottom chart). The only exception observed for Form A1 can be explained by extremely low concentration of the API in the model system that was below 0.5 wt.%.

### 3.6. Comparison with other experimental techniques

Although the above-introduced results have demonstrated the ability of the proposed method to distinguish different amorphous forms of atorvastatin in pure state as well as in the mixtures with filler compounds, the relation between the observed systematic variation of  $V_{14}(^{19}\text{F})$  coefficients and structural changes or molecular arrangement in the amorphous phase was not discovered. That is why we tried to examine capability of  $^{19}\text{F}$  MAS NMR spectra to reflect these structural changes in detail. The evaluation process used here is based on the explicit comparison of  $^{19}\text{F}$  MAS NMR spectra with structurally highly receptive experimental data provided by  $^{13}\text{C}$  CP/MAS NMR, FTIR and XRPD (Fig. 1). These techniques were selected because XRPD data reflect supermolecular structure and long-range periodic order;  $^{13}\text{C}$  CP/MAS NMR spectra provide information about short-range arrangement and overall molecular conformation; and FTIR spectra are sensitive to the changes in molecular structure of the investigated system. However, due to the strong signal overlap and unacceptable experimental time required to record spectra with reasonable signal-to-noise ratio all the measurements were conducted only for the samples of atorvastatin without filler compounds.

In general, there is a limited number of procedures that allow independent comparison of different spectroscopic data. As one of them we propose comparative factor analysis, the method based on the correlation of  $V_{ij}$  scores obtained by factor analysis of individual datasets. Using this procedure, the sets of  $^{13}\text{C}$  CP/MAS NMR spectra, FTIR spectra and XRPD patterns are separately processed at first. Subsequently, the obtained  $V_{ij}$  scores are cross-correlated to search for the clear relationships. Specifically, the factor analysis

of  $^{13}\text{C}$  CP/MAS NMR spectra resulted in nearly the same results as extracted from  $^{19}\text{F}$  MAS NMR data and the obtained correlation plot of  $V_{i3}(^{13}\text{C})$  and  $V_{i4}(^{13}\text{C})$  coefficients provides clear distinction of the prepared drug forms (Fig. 8). We must note that the scores derived from  $^{19}\text{F}$  MAS NMR spectra are in perfect agreement with the scores extracted from  $^{13}\text{C}$  CP/MAS NMR spectra. This fact is clearly demonstrated in  $V_{i4}(^{13}\text{C})$ – $V_{i4}(^{19}\text{F})$  cross-correlation plot (Fig. 9, upper chart). Similarly we analyzed other spectroscopic data, and linear relationships were found also for  $V_{i4}(^{19}\text{F})$  and  $V_{i4}(\text{FTIR})$ ; and  $V_{i4}(^{19}\text{F})$  and  $V_{i7}(\text{XRPD})$  coefficients (Fig. 9, central and bottom chart, respectively). Overall, we performed all possible cross-correlations including entire  $V_{ij}(^{19}\text{F}; ^{13}\text{C}; \text{FTIR}$  and XRPD) scores, but only those involving  $V_{i4}(^{19}\text{F})$  and those exhibiting direct proportion are reported in this contribution. Supporting information including interpretation of the obtained subspectra and singular values can be found in Appendix A.

## 4. Discussion

### 4.1. Structural variability of amorphous atorvastatin

Several studies have revealed the existence of different amorphous forms of pharmaceutical solids depending on the preparation technique (Graeser et al., 2008; Greco and Bogner, 2010; Craig et al., 1999; Heinz et al., 2008; Yu, 2001). So it is not surprising that the different amorphous forms of relatively high-molecular-weight atorvastatin containing several flexible side-chains were simply prepared by different solvent-evaporation processes. Moreover, the differently prepared amorphous forms of atorvastatin, that is still under extensive consideration (An and Sohn, 2009), exhibit significantly different physicochemical properties. Quite recently it has been reported that the intrinsic dissolution rates of different amorphous forms of this API considerably differ from 0.183 to 0.252  $\text{mg min}^{-1} \text{cm}^{-2}$  (Shete et al., 2010). That is why the experimental approaches of exact structural characterization of different solid state forms are still a subject of enormous scientific effort.

The differences between the prepared amorphous forms of atorvastatin can be hardly recognized using conventional physical and spectroscopic techniques. This fact is clearly demonstrated in the recorded experimental spectra ( $^{19}\text{F}$  MAS NMR,  $^{13}\text{C}$  CP/MAS NMR, FTIR and XRPD, Fig. 1) which exhibit only weak spectral variations. Specifically, the structural differences of the amorphous phase of atorvastatin have the smallest impact of on spectral pattern of  $^{19}\text{F}$  MAS NMR spectra. This follows from the fact, that XRPD, FTIR spectroscopy and  $^{13}\text{C}$  CP/MAS NMR probe the whole molecular system (i.e. positions of all atoms, vibration modes of all chemical bonds or global structure of carbon skeleton, respectively), while the  $^{19}\text{F}$  MAS NMR spectra are reflecting only the local structural changes around the site occupied by the fluorine atom.

### 4.2. Distinguishing of amorphous forms of atorvastatin

Recent studies meaning the ability of different analytical techniques to characterize differently prepared amorphous forms of pharmaceutical solids have shown that the most powerful approach is based on the combination of spectral methods with multivariate analysis (Graeser et al., 2008; Heinz et al., 2008). Especially Raman spectroscopy combined with principle component analysis (PCA) is being the most sensitive technique towards structural differences in amorphous samples (Heinz et al., 2008). Unfortunately, the PCA of Raman spectra can be hardly used for the low-dosage products of atorvastatin due to the strong overlap of characteristic vibration bands of the API with the signals of excipients and very low signal-to-noise ratio. That is why we

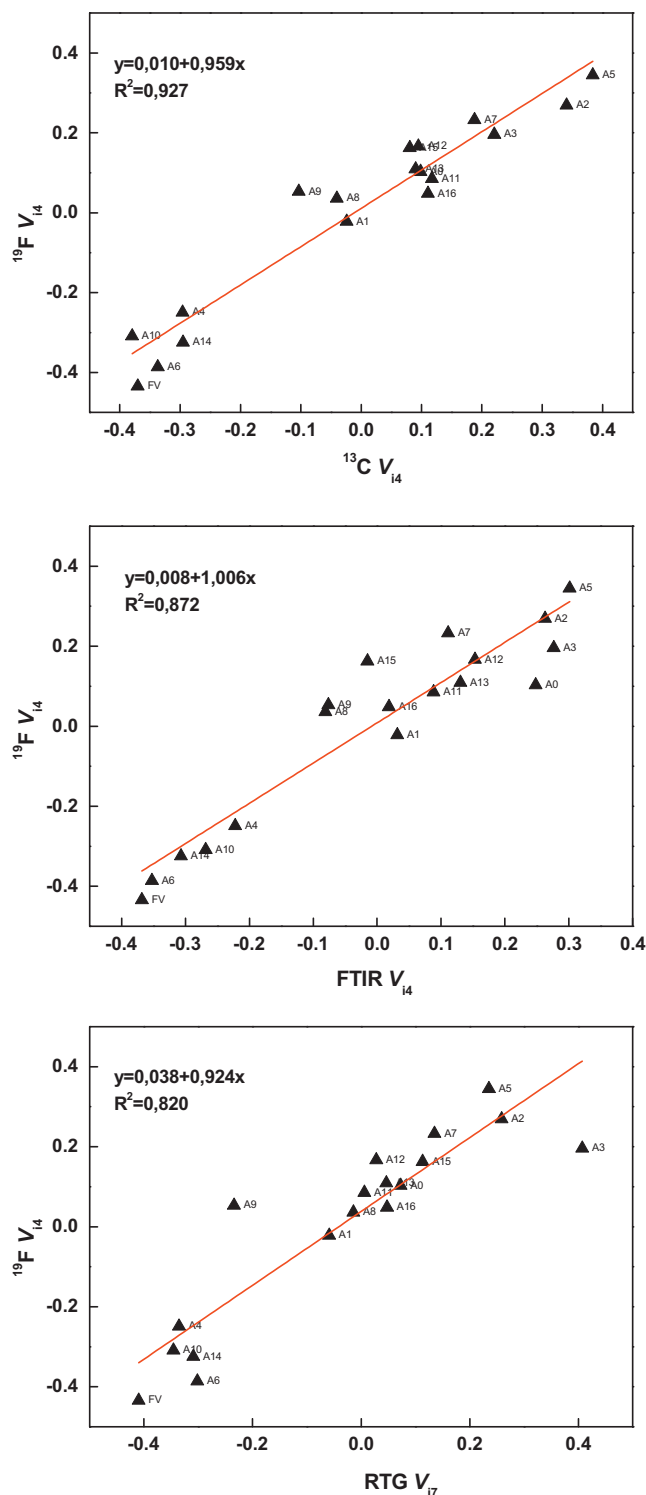


**Fig. 9.** Cross-correlation plots of  $V_{i4}(^{19}\text{F})$ ;  $V_{i4}(^{13}\text{C})$ ;  $V_{i4}(\text{IR})$  and  $V_{i7}(\text{XRPD})$  coefficients characterizing amorphous forms of atorvastatin. Upper chart: cross-correlation of  $V_{i4}(^{19}\text{F})$  and  $V_{i4}(^{13}\text{C})$ ; central chart: cross-correlation of  $V_{i4}(^{19}\text{F})$  and  $V_{i4}(\text{FTIR})$ ; and bottom chart: cross-correlation of  $V_{i4}(^{19}\text{F})$  and  $V_{i7}(\text{XRPD})$  scores.

applied factor analysis on highly sensitive  $^{19}\text{F}$  MAS NMR spectra that can be recorded within short time and in reasonable quality also for the low-dose formulations with atorvastatin. Specifically we used SVD algorithm that has significant advantage over other approaches. Predominantly the applied algorithm produced not only scores characterizing each analyzed sample, but also the subspectra separating specific spectral aspects which can be correlated

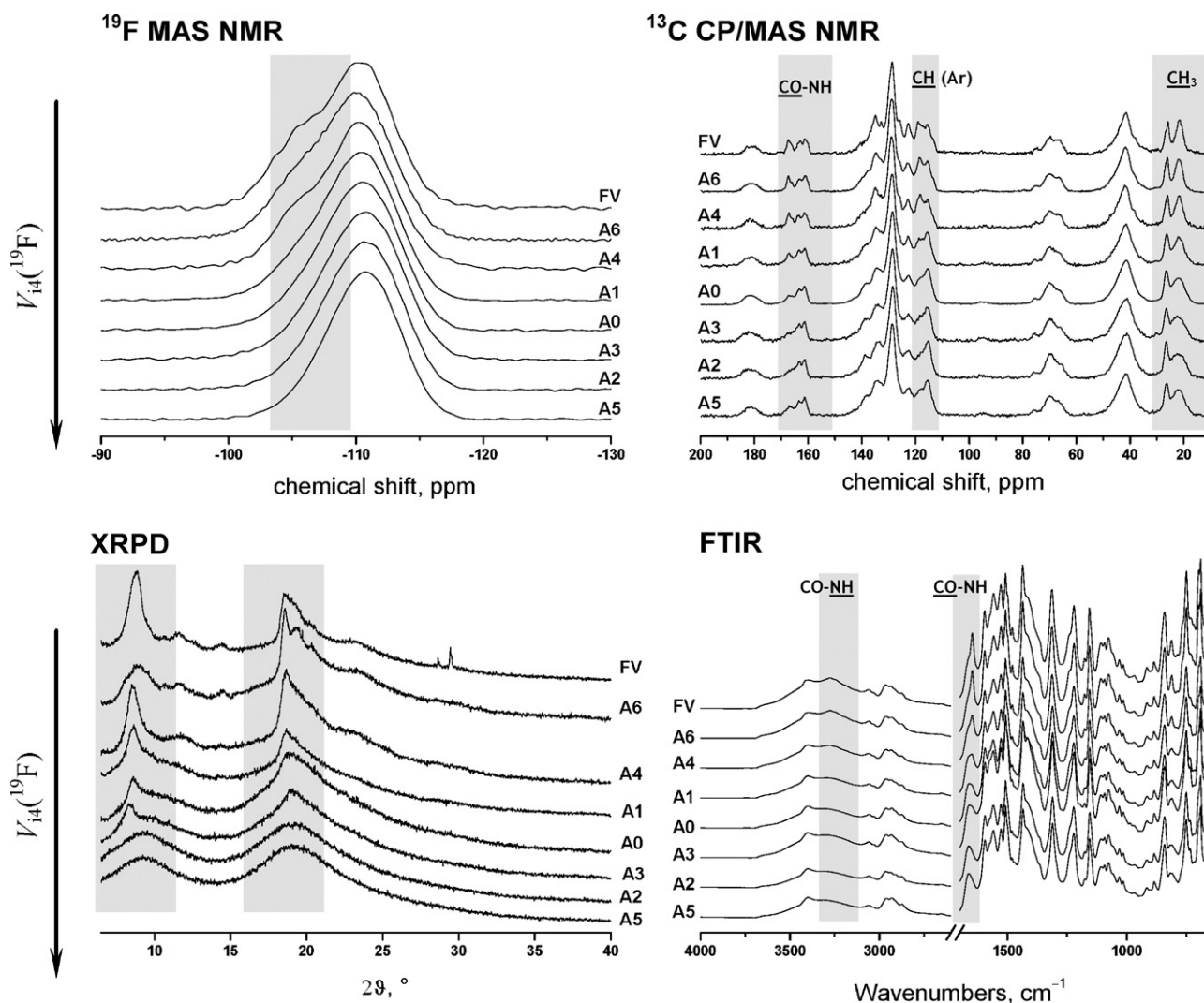


**Fig. 10.** Selected  $^{19}\text{F}$  MAS NMR,  $^{13}\text{C}$  CP/MAS NMR, XRPD patterns and FTIR spectra of representative modifications of atorvastatin. The spectra are assorted in the same order according to the calculated  $V_{i4}(^{19}\text{F})$  coefficients.

with structural changes (Fig. 2). Then according to the obtained subspectra it was easy to find the most suitable scores allowing clear distinction between various amorphous forms of atorvastatin. Because the structural differences between amorphous forms of atorvastatin are relatively subtle then just the scores with a high order can reflect these differences. In our particular case those are 4th-order scores  $V_{i4}(^{19}\text{F})$  which in the most suitable correlation with 3rd-order scores  $V_{i3}(^{19}\text{F})$  allow the differences between the amorphous forms to be clearly observed in vertical dimension (Fig. 3).

All the performed subsequent tests, including analysis of various two-component mixtures as well as estimation of uncertainty in the calculated scores, confirmed sufficient reliability of the proposed approach. Even though the differences in the recorded  $^{19}\text{F}$  MAS NMR spectra are visually barely perceptible, utilizing the factor analysis the different amorphous forms of atorvastatin can be clearly distinguished via the calculated scores. Moreover, the proposed method allows recognizing the mixtures of the prepared forms of atorvastatin with the detection limit of the crystalline phase impurities in amorphous phase less than 1%. The detection of minor fraction of amorphous phase impurities in the matrix of another amorphous form of atorvastatin is, however, much more tricky. The  $^{19}\text{F}$  MAS NMR signals of both components are so similar that neither the computer decomposition of  $^{19}\text{F}$  MAS NMR spectra

does allow clear identification and quantification of these mixtures. The factor analysis, however, is sufficiently powerful to provide reasonable results also in this case, and almost invisible changes in the shape of  $^{19}\text{F}$  MAS NMR spectra of the mixtures can be converted to the consistent changes of the corresponding  $V_{i4}(^{19}\text{F})$  scores with the lowest detection limit being about 5–10%. Admittedly this detection limit is not reached generally, because the differences between  $V_{i4}(^{19}\text{F})$  scores of the pure modifications of atorvastatin forming the mixture must be sufficiently large. For instance, this precondition is fulfilled for the systems consisting of Forms A3 and A6; or Forms V and A5 (Fig. 4). In the opposite cases, when the differences between the scores of pure substances are considerably smaller, the detection limits of minor components correspondingly increase.

From our experience built on the extensive testing, the best way how to utilize the proposed procedure starts with the creation of a reference database of  $^{19}\text{F}$  MAS NMR spectra of pure forms of a given API. Such database should include representative amorphous as well as crystalline modifications. Approximately 10–15 forms of the particular API seem to be enough. When a new sample is analyzed, its  $^{19}\text{F}$  MAS NMR spectrum can be added into the already made dataset. Subsequently performed factor analysis then characterizes this sample via its  $V_{ij}(^{19}\text{F})$  scores. The reference database should be kept constant or nearly constant for all analysis of unknown samples.

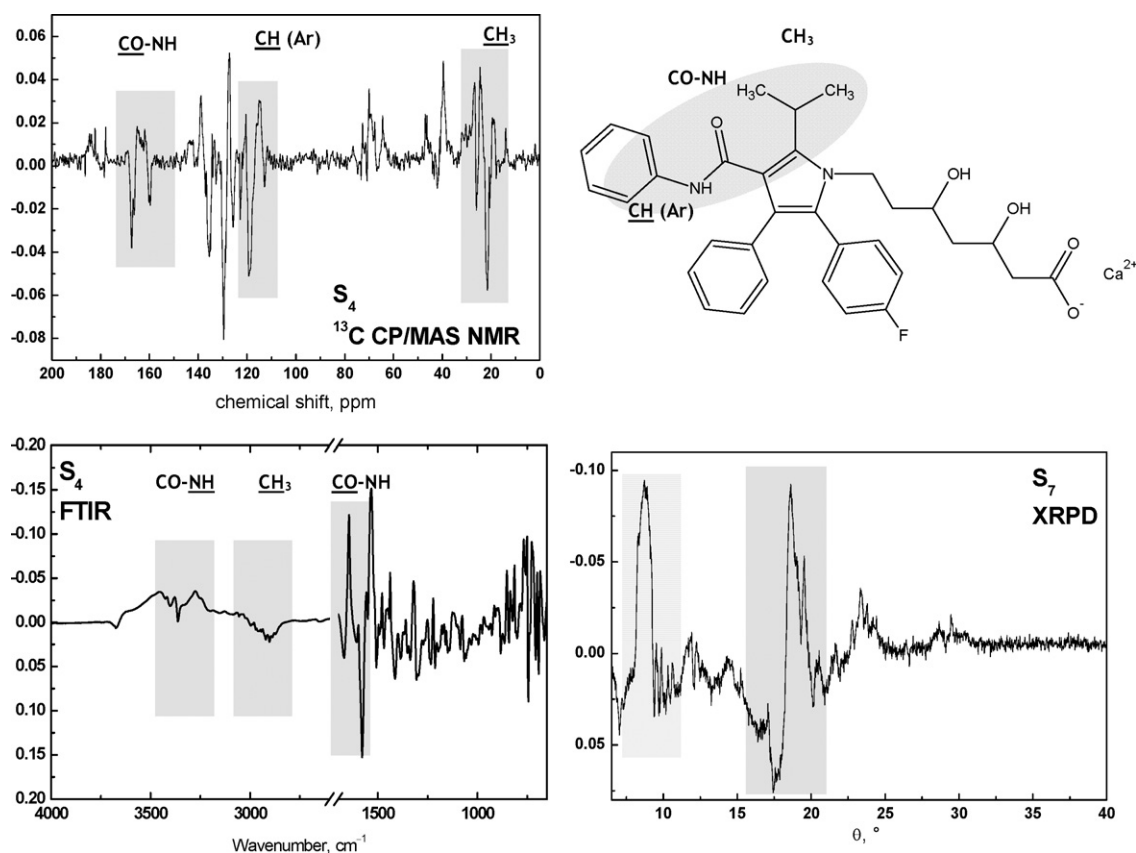


**Fig. 11.** Subspectra  $S_4(^{13}\text{C})$ ,  $S_4(\text{FTIR})$  and  $S_7(\text{XRPD})$  calculated from the representative sets of experimental data of various modifications of atorvastatin. The “high-amplitude” signals assigned to the molecular sites exhibiting substantial structural variability are highlighted.

Similarly, the reference database of different polymorphs must be created also for the API in dosage formulations. Although the filler compounds are thought to be inert, weak interactions with the molecules of the API cannot be excluded. In our case we noticed slight systematic deviation in  $V_{ij}(^{19}\text{F})$  scores obtained for pure forms of atorvastatin from those obtained for the corresponding mixtures with excipient (Fig. 7). Close inspection of the recorded  $^{19}\text{F}$  MAS NMR spectra revealed slight systematic shift of  $^{19}\text{F}$  NMR signals in model mixtures towards higher frequencies. With high probability, this phenomenon can be attributed to the changes in sample susceptibility, because in dosage forms the dielectric properties of the samples are dominated by the excipient.

Despite these problems the proposed method provides routine, fast and reliable tool to distinguish different amorphous forms of atorvastatin even in low-dose tablet formulation. Applying  $^{19}\text{F}$  MAS NMR spectroscopy the high-quality spectra can be recorded within 10–30 min. Consequently the total time to identify an unknown form of atorvastatin in the dosage form is less than 1 h. Therefore the proposed method is considerably timesaving compared with traditionally used  $^{13}\text{C}$  CP/MAS NMR. As recently demonstrated even the one-day acquisition of  $^{13}\text{C}$  CP/MAS NMR spectra of low-dose formulations of levosimendan (<1%) did not allow the clear identification of the present crystalline modification (Virtanen and Maunu, 2010).

#### 4.3. Structural receptivity of $^{19}\text{F}$ MAS NMR spectra

In general, the observed systematic variations of the scores obtained by multivariate analysis of  $^{19}\text{F}$  MAS NMR spectra can result from many reasons including changes in crystallinity, structural transformations, presence of impurities etc. In order to find clear relationships between the molecular structure of atorvas-

tatin and the observed systematic variation of  $V_{i4}(^{19}\text{F})$  scores, the obtained experimental data were compared with the results of other spectroscopic techniques. Specifically, we cross-correlated  $V_{i4}(^{19}\text{F})$  scores with the coefficients obtained by the factor analysis of  $^{13}\text{C}$  CP/MAS NMR, FTIR and XRPD experimental data. A bit surprisingly we found almost perfect linear dependences between  $V_{i4}(^{19}\text{F})$  coefficients and  $V_{i4}(^{13}\text{C})$ ,  $V_{i4}(\text{IR})$ , and  $V_{i7}(\text{XRPD})$  scores. In addition, the absolute values of slopes of these dependences are near to 1 (Fig. 9). This indicates that these scores are of the same significance and the corresponding subspectra ( $S_{i4}(^{19}\text{F})$ ,  $S_{i4}(^{13}\text{C})$ ,  $S_{i4}(\text{FTIR})$ ,  $S_{i7}(\text{XRPD})$ ) are strongly interrelated, describing thus inherent properties of the amorphous phase of atorvastatin.

In general,  $^{19}\text{F}$  MAS NMR,  $^{13}\text{C}$  CP/MAS NMR as well as FTIR spectroscopy all provide site-specific information on the local molecular structure. Therefore it is not surprising that given structural changes of the amorphous phase can be found at the same level, i.e. in the subspectra of the same order. On the other hand, the information which is in the case of NMR and FTIR measurements reproduced in the 4th-order subspectra, is shifted up to the 7th-order subspectrum of XRPD dataset. With high probability this phenomenon can be explained by the fact that XRPD is primarily sensitive on structural changes of crystalline solids. Consequently one can assume that  $S_{i2}$  to  $S_{i6}(\text{XRPD})$  subspectra reflect complex relationships between different crystalline forms of atorvastatin. Weak changes in amorphous phase are then reflected in the higher-order subspectra  $S_{i7}$  to  $S_{i9}(\text{XRPD})$  (Appendix A, A3a and A3b).

#### 4.4. Factor analysis and molecular structure of atorvastatin

As the obtained  $^{19}\text{F}$  MAS NMR spectra can be only hardly interpreted in the terms of molecular arrangement of amorphous atorvastatin, the site-specific information on molecular structure

must be deduced from complementary  $^{13}\text{C}$  CP/MAS NMR, and FTIR spectra and XRPD patterns (Fig. 10). In the  $^{19}\text{F}$  MAS NMR spectra assorted in the descending order according to  $V_{ij}(^{19}\text{F})$  scores the NMR signals exhibit gradual narrowing and symmetrization as the left-hand shoulder disappear. In the corresponding  $^{13}\text{C}$  CP/MAS NMR spectra these changes are associated with the lost of resolution of methyl signals (ca. 20 ppm), signals of  $-\text{CH}=\text{}$  units in aromatic rings (ca. 120 ppm) and  $\text{CO}-\text{NH}-$  carbonyl signals (ca. 160 ppm). The same molecular sites exhibit weak but still perceptible spectral changes also in the corresponding FTIR spectra. These observations thus indicate that structural variability of amorphous forms of atorvastatin is associated with the conformational changes occurring predominantly around these molecular sites. Besides the local structural changes the recorded XRPD data indicate considerable changes in the molecular long-range periodic arrangement of the amorphous phase. In the same order as  $^{19}\text{F}$  MAS NMR signals become symmetrical and narrow, the sharp residual X-ray reflections gradually diminish. This indicates that primary structural motifs of long-range periodic arrangement of the molecules of the API in amorphous phase play considerable role in the formation of amorphous forms of atorvastatin (Fig. 10).

Detail structural information can be directly derived from the subspectra  $S_4(^{13}\text{C})$ ,  $S_4(\text{FTIR})$  and  $S_7(\text{XRPD})$  (Fig. 11). The signals significantly enhanced in their relative amplitudes clearly reflect molecular sites or typical interatomic distances that are most affected by the structural changes in the amorphous phase of atorvastatin. For instance, in  $S_4(^{13}\text{C})$  subspectrum such relative increase in signal intensity is clearly apparent for the signals resonating at ca. 160, 120 and 20 ppm. Oppositely, the signals at ca. 45, 70 and 180 ppm are relatively suppressed. This confirms previous statement that structural changes in amorphous phase of atorvastatin are basically connected with local rearrangement around amide carbonyl and neighboring methyl groups, while the hydroxyl-substituted side-chains and carboxyl unit seem to be structurally unaffected. The great advantage of factor analysis is clearly demonstrated in  $S_4(\text{FTIR})$  subspectrum in which the relative signal enhancement is observed not only for vibration bands of  $\text{CO}-\text{NH}$  groups (ca. 3200 and 1700  $\text{cm}^{-1}$ ) but also for methyl units (ca. 3000  $\text{cm}^{-1}$ ). Moreover, the above-discussed global molecular rearrangement of the molecules of atorvastatin in amorphous phase and the formation of partially ordered assemblies is clearly apparent in  $S_7(\text{XRPD})$  subspectrum. As reflected by the high-amplitude diffraction peaks at  $8^\circ$  and  $20^\circ$   $2\theta$ , the average correlation length typical for these assemblies is about 4 and 11 nm, respectively. Roughly estimated, the mentioned correlation distances can be attributed to some structural motifs of aromatic rings probably involved in  $\pi-\pi$  interactions. Consequently it can be supposed that the amorphous phase of atorvastatin consist of molecular assemblies which build-up is associated with rearrangement of amide groups and stacking of aromatic rings. The individual amorphous forms of atorvastatin then can differ in the extent of such arrangement. However, detail interpretation of the observed phenomena that can be derived from the application of pair distribution function transforms is behind the scope of this contribution and it is currently under investigation.

## 5. Conclusion

Due to the major success of fluorinated compounds in medicinal chemistry, it may be predicted that the number of fluorine containing drugs on the market will continue to increase. Similarly we can expect growing interest in the formulation of APIs in amorphous forms including development of solid solutions and dispersions of APIs in polymer matrix for which, however, traditional high-resolution spectral data can be hardly obtained. Consequently any

attempt to develop a method of detail structural characterization of these amorphous low-dose formulations of APIs is worth of the effort.

In this contribution it was demonstrated that  $^{19}\text{F}$  MAS NMR spectroscopy combined with factor analysis (SVD algorithm) offers a fast, routine and reliable tool to identify disordered and amorphous forms of atorvastatin (representative of fluorine-containing APIs) in both substance itself and low-dose tablet formulations. Specifically, it was shown that even relatively poorly-resolved  $^{19}\text{F}$  MAS NMR spectra can be used to detect subtle differences between various amorphous forms of atorvastatin. Applying the factor analysis on  $^{19}\text{F}$  MAS NMR spectra, the sample-specific coefficients (scores,  $V_{ij}(^{19}\text{F})$ ) characterizing every product can be obtained. In a graphical representation these scores provide clear identification and distinction of different amorphous forms of atorvastatin. The proposed method also offers the ability to identify and quantify various mixtures of different modifications of atorvastatin. Predominantly, however, the proposed method allows the fast characterization of low-dose pharmaceutical products. Applying  $^{19}\text{F}$  MAS NMR spectroscopy the acceptable spectra of tablet formulations containing ca. 1–5% of atorvastatin can be recorded within 10–30 min. Consequently the total time to identify an unknown form of atorvastatin in the dosage form is less than 1 h. In conclusion, the proposed method has at least the ability to reveal deviations from the expected output and thus to unambiguously identify undesired products of manufacture.

Extensive testing of the method based on the comparison with  $^{13}\text{C}$  CP/MAS NMR, FTIR and XRPD data confirmed that the computed  $V_{ij}(^{19}\text{F})$  scores can be considered as structure-related parameters describing changes in molecular arrangement of atorvastatin. This indicates that  $^{19}\text{F}$  MAS NMR spectra can in principle reflect changes in amorphous phase of organic (fluorine-containing) compounds in similar extent as usually provided by the more informative techniques like  $^{13}\text{C}$  CP/MAS NMR, FTIR and XRPD. We note that isotropic NMR shifts are by far the easiest solid-state NMR parameter to measure. That is why the proposed method that does not need NMR signal assignment can be applied to other high-sensitive nuclei like  $^{31}\text{P}$ ,  $^{23}\text{Na}$ ,  $^{11}\text{B}$  etc. While absent in filler compounds these nuclei are common components of many pharmaceutical compounds. Our work thus extends the application of solid-state NMR spectroscopy in the field of qualitative and quantitative characterization of amorphous pharmaceutical solids in low-dose formulations. The excellent results presented here have encouraged further work to test the general applicability of the proposed method to describe structural motifs in amorphous phase pharmaceutical solids, which is underway.

## Acknowledgement

Funding from Ministry of Education, Youth and Sports of the Czech Republic (research program 2B08021) is acknowledged.

## Appendix A. Supplementary data

Supplementary data associated with this article can be found, in the online version, at doi:10.1016/j.ijpharm.2011.02.030.

## References

- An, S.-G., Sohn, Y.-T., 2009. Crystal forms of atorvastatin. Arch. Pharm. Res. 32, 933–936.
- Aronhime, J., Lidon-Hadas, R., Niddam, V., Lifshitz, R., 2003. Atorvastatin hemicalcium form VII. US Patent 6605636 (12.8.2003).
- Aronhime, J., Lifshitz, R., Niddam, V., Lidon-Hadas, R., Wizel, S., 2006. Novel crystal forms of atorvastatin hemicalcium and processes for their preparation as well as novel processes for preparing other forms. US Patent 7144916 (5.12.2006).

- Aso, Y., Yoshioka, S., Miyazaki, T., Kawanishi, T., 2009. Feasibility of  $^{19}\text{F}$ -NMR for assessing the molecular mobility of flufenamic acid in solid dispersions. *Chem. Pharm. Bull.* 57, 61–64.
- Ayalon, A., Levinger, M., Royblat, S., Niddam, V., Lifshitz, R., Aronhime, J., 2008. Polymorphic form of atorvastatin calcium. US Patent 7411075 (12.8.2008).
- Bauer, J., Spanton, S., Henry, R., Quick, J., Dziki, W., Porter, W., Morris, J., 2001. Ritonavir: an extraordinary example of conformational polymorphism. *Pharm. Res.* 18, 859–866.
- Blagden, N., de Matas, M., Gavan, P.T., York, P., 2007. Crystal engineering of active pharmaceutical ingredients to improve solubility and dissolution rate. *Adv. Drug Deliv. Rev.* 59, 617–630.
- Briggs, C.A., Jennings, R.A., Wade, R., Harasawa, K., Ichikawa, S., Minohara, K., Naskagawa, S., 1999. Warner Lambert Co. US Patent 5969156 (19.10.1999).
- Brus, J., 2000. Heating of samples induced by fast magic-angle spinning. *Solid State Nucl. Magn. Reson.* 16, 151–160.
- Brus, J., Jedorov, A., 2004. Through-bonds and through-space solid-state NMR correlations at natural isotopic abundance: signal assignment and structural study of simvastatin. *J. Phys. Chem. A* 108, 3955–3964.
- Claydenaq, N.J., Lehnertb, R.J., Tumocka, S., 1997. Factor analysis of time domain NMR data: crystallinity of poly(tetrafluoroethylene). *Anal. Chim. Acta* 344, 261–269.
- Craig, D.Q.M., Royall, P.G., Kett, V.L., Hopton, M.L., 1999. The relevance of the amorphous state to pharmaceutical dosage forms: glassy drugs and freeze dried system. *Int. J. Pharm.* 179, 179–207.
- Eads, C.D., Furnish, C.M., Noda, I., Juhlin, K.D., Cooper, D.A., Morrall, S.W., 2004. Molecular factor analysis applied to collections of NMR spectra. *Anal. Chem.* 76, 1982–1990.
- Gogulapati, V.P.R., Chavakula, R., Bandami, M., Gorantla, S.R., 2004. Crystalline form of atorvastatin hemi-calcium. US Patent 20090240064 (24.09.2004).
- Graeser, K.A., Strachan, C.J., Patterson, J.E., Gordon, K.C., Rades, T., 2008. Physico-chemical properties and stability of two differently prepared amorphous forms of simvastatin. *Cryst. Growth Des.* 8, 128–135.
- Greco, K., Bogner, R., 2010. Crystallization of amorphous indomethacin during dissolution: effect of processing and annealing. *Mol. Pharm.* (on-line publication: 13.5.2010).
- Griffin, J.M., Martin, D.R., Brown, S.P., 2007. Distinguishing anhydrous and hydrated forms of an active pharmaceutical ingredient in a tablet formulation using solid-state NMR spectroscopy. *Angew. Chem. Int. Ed.* 46, 8036–8038.
- Harris, R.K., 2006. NMR studies of organic polymorphs & solvates. *Analyst* 131, 351–373.
- Harris, R.K., Cadars, R., Emsley, L., Yates, J.R., Pickard, C.J., Jettid, R.K.R., Griesserd, U.J., 2007. NMR crystallography of oxybuprocaine hydrochloride. *Modification II<sup>o</sup>*. *Phys. Chem. Chem. Phys.* 9, 360–368.
- Harris, R.K., 2007. Applications of solid-state NMR to pharmaceutical polymorphism and related matters. *J. Pharm. Pharmacol.* 59, 225–239.
- Heinz, A., Strachan, C.J., Atassi, F., Gordon, K.C., Rades, T., 2008. Characterizing an amorphous system exhibiting trace crystallinity: a case study with saquinavir. *Cryst. Growth Des.* 8, 119–127.
- Heinz, A., Gordon, K.C., McGoverin, M.C., Rades, T., Strachan, C.J., 2009. Understanding the solid-state forms of fenofibrate – a spectroscopic and computational study. *Eur. J. Pharm. Biopharm.* 71, 100–108.
- Henry, E.R., Hofrichter, J., 1992. Singular value decomposition: application to analysis of experimental data. *Methods Enzymol.* 210, 129–192.
- Husak, M., Jedorov, A., Brus, J., Beek, van W., Patison, P., Christensen, M., Favre-Nicolin, V., Maixner, J., 2008. Metergoline II: structure solution from powder diffraction data with preferred orientation and from microcrystal. *Struct. Chem.* 19, 517–525.
- Husak, M., Kratochvil, B., Jedorov, A., Brus, J., Maixner, J., Rohlíček, J., 2010. Simvastatin: structure solution of two new low-temperature phases from synchrotron powder diffraction and ss-NMR. *Struct. Chem.* 21, 511–518.
- Koonst, J.M., Ellis, P.D., 1995. Applicability of factor analysis in solid state NMR. *Anal. Chem.* 67, 4309–4315.
- Levine, B.K., 1998. *Chemometrics*. *Anal. Chem.* 70, 209–228 (Review).
- Purser, S., Moore, P.R., Swallow, S., Gouverneur, V., 2008. Fluorine in medicinal chemistry. *Chem. Soc. Rev.* 37, 320–330.
- Shete, G., Puri, V., Kumar, L., Bansal, A.K., 2010. Solid state characterization of commercial crystalline and amorphous atorvastatin calcium samples. *J. Pharm. Sci. Technol.* 11, 598–609.
- Tessler, L., Aronhime, J., Lifshitz, R., Maidan-Hanoch, D., Hasson, N., 2008. Novel crystal forms of atorvastatin hemi-calcium and processes for their preparation as well as novel processes for preparing other forms. US Patent 7456297 (25.11.2008).
- Virtanen, T., Maunu, S.L., 2010. Quantitation of a polymorphic mixture of an active pharmaceutical ingredient with solid state  $^{13}\text{C}$  CPMAS NMR spectroscopy. *Int. J. Pharm.* 394, 18–25.
- Yu, L., 2001. Amorphous pharmaceutical solids: preparation, characterization and stabilization. *Adv. Drug Deliv. Rev.* 48, 27–42.
- Zakrzewski, A., Zakrzewski, M., 2006. *Solid State Characterization of Pharmaceuticals*. Pergamon.